

TNO Defence Research

TNO Prins Maurits Laboratory

TD

Lange Kleiweg 137
P.O. Box 45
2280 AA Rijswijk
The Netherlands

Fax +31 15 84 39 91
Telephone +31 15 84 28 42

92-3686
①

AD-A274 154



TNO-report
PML 1992-128

June 1993
Copy no.: 16

Description and validation of an improved
frangible armour piercing munition model

S DTIC
ELECTE
DEC 27 1993
A

Author(s)

T. Keij

DO-assignment no

A91/KI/422

*Original contains color
plates: All DTIC reproductions
will be in black and
white*

Classification

Report

ONGERUBRICEERD

Title

ONGERUBRICEERD

Summary

ONGERUBRICEERD

Annex(es)

ONGERUBRICEERD

93-31051
Barcode

Number of copies

33

Number of pages

(incl. annexes), excl. distr. list and POP

48

Number of Annexes

2

The classification designation:

ONGERUBRICEERD

is equivalent to:

UNCLASSIFIED

This document has been approved
for public release and sale, its
distribution is unlimited

All rights reserved.
No part of this publication may be
reproduced and/or published by print,
photoprint, microfilm or any other means
without the previous written consent of
TNO.

In case this report was drafted on
instructions, the rights and obligations of
contracting parties are subject to either the
'Standard Conditions for Research
Instructions given to TNO', or the relevant
agreement concluded between the
contracting parties.
Submitting the report for inspection to
parties who have a direct interest is
permitted.

© TNO

All information which is classified according to Dutch regulations shall be
treated by the recipient in the same way as classified information of
corresponding value in his own country.
No part of this information may be disclosed to any party.

93 12 22 1 64

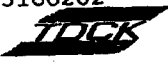
Netherlands organization for
applied scientific research

TNO Defence Research consists of:
the TNO Physics and Electronics Laboratory,
the TNO Prins Maurits Laboratory and the
TNO Institute for Perception



TDCK

Frederikkazerne, gebouw 140
v/d Burchlaan 31 MPC 16A
TEL. : 070-3166394/6395
FAX. : (31) 070-3166202
Postbus 90701
2509 LS Den Haag



**Best
Available
Copy**

Summary

Frangible Armour Piercing Discarding Sabot (FAPDS) munition is a new type of medium calibre munition for air defense systems. Its penetration behaviour has been studied by TNO-PML in cooperation with BWB, IABG, and Rheinmetall. These studies lead to a simulation model describing the penetration behaviour of 35 mm FAPDS projectiles in thin plate arrays.

This report discusses an improved version of the semi-empirical terminal ballistics model for FAPDS munition. With regard to the first simulation model (as reported in report PML 1992-6), the characteristics of the fragmentation process have been changed (use of Mott distribution instead of random distribution, increase in number of particles, and decrease in scattering angle), and the parasitic effect has been described more accurately (effect of hole and particle size on penetration behaviour is included). Due to the changes in the model, the simulation results are consistent with the experimental results. Now, the maximum penetration capacity and the fragment beam width can be calculated accurately for 35 mm FAPDS munition. The influence of the target array composition and the rifling twist of the gun on the simulation results can also be predicted well.

However, some problems still have to be solved before the terminal ballistics model can be incorporated into a vulnerability assessment code. The major problem is finding a way to deal with synergistic effects. It is expected that the problems will be solved within the next half year, so that effectiveness calculations can be performed against aircraft and helicopters. The calculation results will be used for the evaluation of several munition types as replacement of today's munition for air defense systems.

Samenvatting

Frangible Armour Piercing Discarding Sabot (FAPDS) munitie is een nieuw type middenkaliber munitie voor luchtverdedigingssystemen. Het penetratiegedrag van dit type munitie is door PML-TNO in samenwerking met BWB, IABG en Rheinmetall bestudeerd. Deze studies hebben geresulteerd in een simulatiemodel dat het penetratiegedrag van 35 mm FAPDS projectielen in dunne platenarrays beschrijft.

Dit rapport geeft een beschrijving van een verbeterde versie van het semi-empirische eindballistische model voor FAPDS munitie. Ten opzichte van de eerste versie van het simulatiemodel (zie rapport PML 1992-6) zijn in de verbeterde versie de eigenschappen van het verschervingsproces aangepast (gebruik van een Mott verdeling in plaats van een random

verdeling, grotere aantallen scherven en een kleinere spreidingshoek) en is de beschrijving van het parasitaire effect verbeterd (het effect van de scherf- en gatgrootte op het penetratiegedrag wordt in rekening gebracht). Door deze veranderingen komen de simulatieresultaten overeen met de experimentele resultaten. De maximale penetratiecapaciteit en de bundelbreedte kunnen voor 35 mm FAPDS munitie nauwkeurig worden berekend. Bovendien zijn de invloed van de doelsamenstelling en van de spoed van het kanon op de resultaten goed te beschrijven met het model.

Er zijn echter nog enkele problemen die de implementatie in een kwetsbaarheidscode bemoeilijken. Het grootste probleem wordt veroorzaakt door het synergetisch effect. De problemen zullen naar verwachting binnen een half jaar worden opgelost, zodat effectiviteitsberekeningen tegen vliegtuigen en helicopters kunnen worden uitgevoerd. De resultaten van deze berekeningen zullen worden gebruikt bij de evaluatie van verschillende typen munitie voor de luchtverdediging.

DTIC REPORT NUMBER 6

Author	
Title	
Abstract	
Keywords	
Availability	
Ordering	
Dist	
A-1	

CONTENTS

	SUMMARY/SAMENVATTING	2
	CONTENTS	4
1	INTRODUCTION	5
2	THE 35 MM FAPDS PROJECTILE	7
3	THE FAPDS SIMULATION MODEL	8
3.1	The penetration model	8
3.2	The fragmentation model	11
3.3	The parasitism model	13
3.4	The FAPDS simulation computer program	13
4	VALIDATION OF THE FAPDS SIMULATION MODEL	16
4.1	FAPDS simulation results	16
4.2	Influence of target composition and rifling twist	25
4.3	Influence of parameters of the simulation model on the results	26
5	THE IMPLEMENTATION OF THE FAPDS SIMULATION MODEL IN A VULNERABILITY ASSESSMENT CODE	29
6	CONCLUSIONS	31
7	AUTHENTICATION	31
8	REFERENCES	32
9	LIST OF SYMBOLS	34
ANNEX A	THE MODIFIED THOR EQUATIONS	
ANNEX B	THE FAPDS SIMULATION COMPUTER PROGRAM	

1 INTRODUCTION

One of the new medium calibre munition types is the so-called Frangible Armour Piercing Discarding Sabot (FAPDS) munition. The FAPDS round consists of a sub-calibre projectile, which may comprise a frangible core enclosed by a steel nose and a tungsten rear part. The frangible part is meant to continuously break up during penetration of the target and to generate a fragment beam. The fragment beam gives an axial as well as a radial damage pattern.

FAPDS munition has, as a sub-calibre projectile, a low time-of-flight and therefore relatively high hit probability and, because of its design, can defeat different kinds of targets, i.e. soft material targets such as aircraft, and lightly armoured targets such as helicopters and personnel carriers.

The Bundesamt für Wehrtechnik und Beschaffung (BWB) and the Rheinmetall company have been performing experiments to study the penetration behaviour of the FAPDS projectile. However, no satisfactory description has as yet been found to describe the penetration process. Such a physical description is necessary to develop a penetration model that can be incorporated into vulnerability assessment codes.

In 1986, TNO-PML was asked by Directie Materieel Koninklijke Landmacht, afdeling Munitie (DMKL) to contribute to the development of a physical description of the FAPDS projectile behaviour. This was done in cooperation with the BWB, the Industrieanlagen Betriebsgesellschaft (IABG) and Rheinmetall.

Since 1987, TNO has been performing an extensive experimental programme [1,2] to study the terminal ballistics of the FAPDS munition. The study has concentrated on a concept of Rheinmetall. Experiments on multiple plate arrays have led to a better qualitative understanding of the 35 mm FAPDS munition penetration behaviour. As a result, quantifications of effects involved in the penetration process could be made [3,4].

In the second phase of the study, started in June 1991, special attention was paid to the modelling of the terminal ballistics behaviour of FAPDS munition for vulnerability assessment studies. The incorporation of such a model into vulnerability assessment codes is rather complicated, as indicated below.

In ordinary vulnerability assessment codes, such as the TNO-PML TARget Vulnerability Assessment Code (TARVAC), the projectile trajectory is simulated by a single (straight) line which is traced through the target. Along this line, calculations are performed to determine the

extent of the projectile's penetration into the target and the damage inflicted upon the target. This approach leads to satisfactory results for single projectile munition types.

In contrast, the FAPDS munition desintegrates into many fragments or particles¹ which penetrate the target more or less simultaneously, while the fragments continuously break up into little particles whenever they hit some part of the target. Therefore, simulation of the projectile trajectory with a single shot line is not sufficient. A shot line should be evaluated for each fragment. Furthermore, the effects produced by the individual fragments are not independent for two reasons.

- 1 Whenever a fragment creates a hole in the target, another fragment which arrives at a later time can fly straight through the hole. The latter does not need to perforate the target again, and hence will not break up. This effect is referred to as parasitism.
- 2 The impact of multiple fragments can give a greater effect than an equal number of fragments hitting the target separately. In other words, the total effect will be greater than the sum of the parts due to synergism.

A first approach for an FAPDS simulation model to describe the penetration behaviour of 35 mm FAPDS projectiles into thin plate arrays was presented in [5]. In the mean time, the FAPDS simulation model has been improved, and some aspects have been studied in greater detail. This report discusses the improved simulation model.

The simulation model is valid for the FAPDS round under development, which is presented in Chapter 2. In Chapter 3, a full description of the improved FAPDS simulation model is presented. The comparison of the results achieved with the simulation model with the experimental results is discussed in Chapter 4, as well as the influence of certain model parameters on the simulation results. Finally, the problems related to the implementation of the simulation model in a vulnerability assessment code are discussed in Chapter 5.

It is expected that these problems will be solved within the next half year, so eventually calculations can be performed against aircraft and helicopters. The calculation results will be used for the evaluation of several munition types as replacement of today's munition for air defence systems.

1 We will use the words "fragments" and "particles" to indicate the difference between respectively the fragments before and after breaking up.

2 THE 35 MM FAPDS PROJECTILE

The FAPDS simulation model has been validated for the 35 mm FAPDS round under development, which comprises a frangible core enclosed by a steel nose and a tungsten rear part. This munition was produced by Rheinmetall. A cross-section of the projectile is shown in Figure 1.

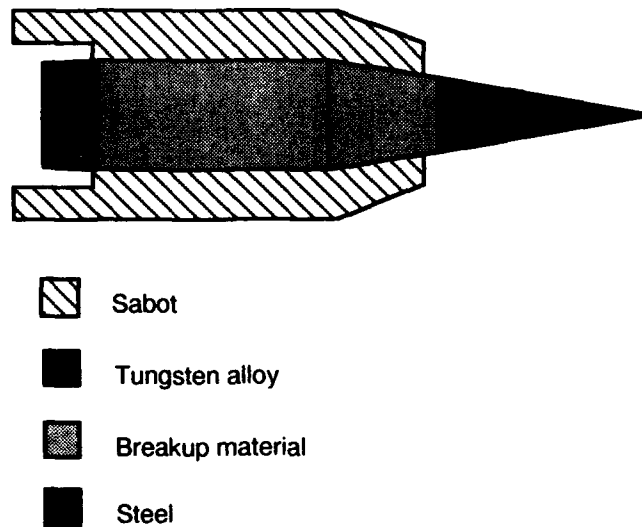


Figure 1 35 mm FAPDS projectile (penetrator and sabot)

At this moment, also different kinds of FAPDS projectiles (e.g. projectiles completely made of frangible material) are available. Even different calibre FAPDS rounds (e.g. 25 mm) are being produced. The FAPDS simulation model has not been validated for these projectiles yet.

3 THE FAPDS SIMULATION MODEL

On the basis of the experimental results [1,2,3,6], an FAPDS simulation model has been developed. This model describes the penetration behaviour of 35 mm FAPDS projectiles into thin plate arrays.

The FAPDS simulation model is a cascade model; the frangible part of the projectile will break up on target impact, and each fragment breaks up into smaller particles at each subsequent target plate encounter. The perforation process of a target plate is divided into two successive steps; the penetration of the target plate, and the breaking up of a fragment after perforation. A penetration model is used to determine the residual mass and velocity of the fragments after perforation of the target plate. A fragmentation model is used to calculate mass, velocity and spatial distributions for the particles into which a fragment breaks up. Finally, a model to account for the effect of parasitic fragments is included in the FAPDS simulation model.

The synergistic effect is not included in the simulation model. However, an estimate of the synergistic effect will be made while evaluating the simulation results (Chapter 4).

The respective models, which form together the FAPDS simulation model, are described below. The models have been implemented in an FAPDS simulation computer program. This computer program is discussed at the end of this chapter.

3.1 The penetration model

In the FAPDS simulation model the so-called THOR equations are used to calculate the residual mass and velocity of the fragments after penetration of a target plate. The equations are also used to describe the penetration of the nose and rear part of the FAPDS projectile. However, these parts will not break up after perforation of the target.

The THOR equations were derived experimentally from ballistic tests [7] and will be discussed briefly.

Consider the configuration shown in Figure 2.

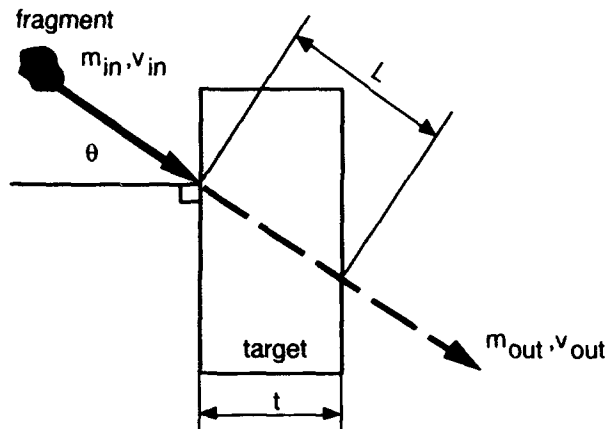


Figure 2 A fragment penetrating a target

A fragment with mass m_{in} and velocity v_{in} hits the target. The angle between the velocity vector of the fragment and the normal of the target surface is defined as θ . During the penetration, the velocity of the fragment as well as its mass reduces. If the fragment strikes the target with sufficient energy, it will perforate¹ the target. The residual mass m_{out} and velocity v_{out} can be calculated with aid of the following THOR equations:

$$v_{out} = v_{in} - 10^{C1} \cdot (t \cdot A)^{C2} \cdot m_{in}^{C3} \cdot \left(\frac{1}{\cos \theta} \right)^{C4} \cdot v_{in}^{C5} \quad (3.1)$$

$$m_{out} = m_{in} - 10^{K1} \cdot (t \cdot A)^{K2} \cdot m_{in}^{K3} \cdot \left(\frac{1}{\cos \theta} \right)^{K4} \cdot v_{in}^{K5} \quad (3.2)$$

where $C1..C5$ and $K1..K5$ are material constants

t = target thickness

A is the average presented area of the fragment calculated from the shape factor S and the mass m_{in} :

$$A = S \cdot m_{in}^{2/3} \quad (3.3)$$

¹ We use the word "perforate" to indicate that a fragment is capable of penetrating a target plate completely, and the residual mass and velocity of the fragment are greater than zero.

If, as result of equations 3.1 and 3.2, the residual mass or velocity is less than or equal to zero, the fragment is not capable of perforating the target.

Since within the beam a velocity gradient is present, a finite probability exists that a fragment encounters a hole in a target plate, created by a fragment arrived earlier. Depending on the dimensions of the fragment and of the hole, the fragment can fly through that hole without any interaction with the target plate (parasitism).

If the fragment is larger than the hole encountered, it will interact with the target plate and it will break up. We have derived modified THOR equations to calculate the residual mass and velocity of the fragments for this specific situation. An extensive description, as well as the derivation, of the modified THOR equations can be found in Annex A.

The principle of these equations will be explained briefly. The equations are based on energy conservation laws. First of all, we calculate the minimum energy necessary to create the hole in the target plate. This minimum energy is added to the residual energy of the fragment necessary to perforate the same target plate without a hole. From the resulting energy, the residual mass and velocity of the fragment is deduced. The original THOR equations (3.1 and 3.2) are applied to calculate the minimum energy, and to deduce the residual mass and velocity.

An important restriction of the modified THOR equations is that they can be used only for small impact angles. However, this is hardly a problem for FAPDS simulations, because the fragments are limited to a narrow cone (Chapter 4).

Another important parameter needed for the FAPDS simulation is the perforation time Δt . The perforation time represents the time it will take a fragment to perforate the target. The principle of constant force is applied in the simulation model to calculate the perforation time. On the basis of the momentum and energy conservation laws (3.4 and 3.5), we arrive at the following expression (3.6) for the perforation time:

$$m_{in} * v_{in} - m_{out} * v_{out} = \int_0^{\Delta t} F * dt = F * \Delta t \quad (3.4)$$

$$1/2 m_{in} * v_{in}^2 - 1/2 m_{out} * v_{out}^2 = \int_0^L F * ds = F * L \quad (3.5)$$

$$\Delta t = \frac{L * (m_{in} * v_{in} - m_{out} * v_{out})}{(1/2 m_{in} * v_{in}^2 - 1/2 m_{out} * v_{out}^2)} \quad (3.6)$$

where F = Force

L = Line-of-sight thickness

3.2 The fragmentation model

Because quantitative theories governing the fragmentation process have not been developed yet, we have used experimental results to obtain the spatial, the fragment mass and the velocity distributions. In addition, experiments with frangible Fragment Simulating Projectiles (FSPs) are planned to obtain more information on the fragmentation of individual fragments.

The elements of the fragmentation model are described below.

Mass distribution

We have assumed that a single fragment (mass m) breaks up according to a Mott distribution into N_0 smaller particles (masses m_i , $i \in [1, N_0]$). The Mott distribution is a cumulative distribution, and is defined by equation 3.7.

$$N(m_i) = N_0 * \exp\left(-\frac{m_i}{0.5 * \bar{m}}\right)^{\frac{1}{2}} \quad (3.7)$$

where $N(m_i)$ = cumulative number of fragments with a mass larger than or equal to m_i

\bar{m} = average fragment mass (= m / N_0)

The total mass of the particles should be equal to the original fragment mass:

$$\sum_{i=1}^{N_0} m_i = m \quad (3.8)$$

Experiments [2] indicate that the number of particles into which a fragment breaks up, ranges from 10 to 20.

Velocity and spatial distribution

After breaking up, the resulting particles travel with different velocities (\bar{v}_i , $i \in [1, N_0]$), both in magnitude and in direction. In the simulation model, the magnitude of the velocity has been chosen equal for all particles originating from one fragment. The velocity of the particles is equal to the residual velocity of the fragment as calculated with the (modified) THOR equations.

The difference in direction is accounted for by a scattering angle α_j :

$$\cos \alpha_j = \frac{\bar{v}_i \cdot \bar{v}}{|\bar{v}_i| \cdot |\bar{v}|} \quad (3.9)$$

where \bar{v} is the velocity vector of the original fragment before break up.

The scattering of the individual particles is limited to a narrow cone (aperture angle about 3 degrees) [2]. The simulation model uses a normal distribution for the scattering of the particles within this cone.

The rifling twist of the gun, from which the FAPDS round is fired, causes the projectile to spin. The spin rate has great influence on the spatial scattering of the particles [6]. The spin rate (ω) of the projectile (diameter D) depends on the rifling twist (RT), the calibre C , and the muzzle velocity v_0 according to:

$$\omega = \frac{\tan(RT)}{(C/2)} \cdot v_0 \quad (3.10)$$

A particle which breaks off from the frangible part of the original projectile can be imparted a maximum tangential velocity ($v_{t \max}$) equal to:

$$v_{t \max} = \omega \cdot \frac{D}{2} = \tan(RT) \cdot v_0 \cdot \frac{D}{C} \quad (3.11)$$

At random, a fraction of the maximum tangential velocity is added to the particle velocity in the simulation model. For particles originating from the original projectile, a first order estimate can be made for the contribution of the tangential velocity to the scattering. The maximum scattering angle (α_{\max}) is given by equation (3.12).

$$\tan(\alpha_{\max}) \approx \frac{v_{t,\max}}{v_0} = \tan(RT) * \frac{D}{C} \quad (3.12)$$

$$\alpha_{\max} \approx RT * \frac{D}{C}, \text{ for small values of } RT \quad (3.13)$$

Equation (3.13) shows that an increase in rifling twist will lead to a proportional increase in scattering angle. As a result, the fragment beam will become wider.

For the 35 mm FAPDS round under study, the following data have been used [6]:

D	= 18 mm
Calibre	= 35 mm
RT	= 6°

As a result, the maximum scattering angle (α_{\max}) will be about three degrees.

3.3 The parasitism model

As stated before, penetrating fragments create holes which will allow other fragments to fly through the target without interactions. The simulation model detects whether a fragment flies through an existing hole. If the fragment is smaller than the hole, it will fly through that hole. If the fragment is larger than the hole, the fragment is not classed as being parasitic. Hence, it will break up after perforation.

3.4 The FAPDS simulation computer program

The models discussed have been implemented in an FAPDS simulation computer program. The program is capable of performing a complete simulation loop, given a normal impact of a 35 mm FAPDS projectile on a thin plate array. As a result of the simulation, a list with holes is generated which yields the damage inflicted upon the target. Furthermore, statistical information on the

fragments can be evaluated (e.g. mass distribution). The information will be used to compare the simulation results with the experimental results (Chapter 4).

Two major mechanisms determine the structure of the FAPDS simulation computer program: the breaking up of the fragments after each perforation and the effect of parasitic fragments.

The breaking up is simulated by creating a new set of vectors after each penetration. Each vector represents a single shot line. The intersections of the shot lines with the target (geometrical model) are calculated with the aid of ray-tracing techniques.

The effect of parasitic fragments implicates a time relation among the fragments. As a result, the time-element must be incorporated in the simulation. We have chosen to make the simulation event-driven. In this approach, each impact of a fragment on the target is regarded as an event. All events are stored in an event list. The first event in the simulation loop is the impact of the original projectile. The event list is empty if no fragments, which are capable of perforating the target, are left. Then, all fragments are stopped within the target or have left the plate array at a side.

The parasitism model itself is implemented through the maintenance of a list with holes. A new hole is added to the list each time a fragment perforates the target. A hole is simply described by a hollow cylinder in the target. The radius r of the cylinder is calculated from the average presented area (A) of the fragment:

$$A = S * m^{2/3} \quad (3.14)$$

and

$$A = \pi * r^2 \quad (3.15)$$

Combining equations 3.14 and 3.15, the radius of the cylinder equals:

$$r = \sqrt{\frac{S * m^{2/3}}{\pi}} \quad (3.16)$$

To determine whether a fragment flies through a hole, the list with holes is scanned until a hole is found for which the impact location on the target is located within the cylinder. If the presented area of the fragment is larger than the hole area, the hole size will be adapted if the modified

THOR equations predict that the relevant fragment is capable of perforating the target. If no hole is found, a new hole is added to the list for that fragment if the relevant fragment is capable of perforating the target.

The complete structure of the FAPDS simulation program and some details on the evaluation of individual events are described in Annex B.

The main assumptions and restrictions of the computer program regarding the various models are summarized below.

Penetration model:

- The (modified) THOR equations can be used to describe the penetration process for all fragments, and for the main parts of the FAPDS projectile.
- The FAPDS projectile strikes the target (thin plate array) perpendicularly.
- The shape factor is equal for all fragments.
- The effect of tumbling is ignored, as well as air drag.
- The hole size is equal to the presented area of the fragment that created the hole.

Fragmentation model:

- Except for the parasitic fragments, each fragment which perforates the target breaks up into a number of particles according to a Mott distribution. The actual number is drawn randomly out of a range, which can be defined by the user.
- After a fragment is broken up, the magnitude of the velocity is equal for all particles.
- The spatial distribution of the scattering angle is normal. The maximum scattering angle can be defined by the user.
- The spin of the original FAPDS projectile is lost after the first fragmentation.

Overall:

- All events are regarded to be independent (except for parasitism effects), meaning no collisions or synergistic effects are included.

4 VALIDATION OF THE FAPDS SIMULATION MODEL

To validate the FAPDS simulation model and its implementation, the results of the experimental programme performed by TNO-PML have been used [1,2]. The experiments were conducted with 35 mm FAPDS projectiles against the so-called TNO-arrays. The TNO-array consists of aluminium plates; the first plate is 8 mm thick, all other plates are 2 mm thick. All plates are placed normal to the line-of-fire at a mutual distance of 30 cm. In the experiments up to seven plates were used for the TNO-array.

The simulation and the experimental results are compared in the first part of this chapter. In the second part, we demonstrate the influence of target composition and rifling twist on the results. Finally, the influence of certain parameters of the simulation model on the results is discussed.

4.1 FAPDS simulation results

The FAPDS simulation computer program has been used to perform simulations of 35 mm FAPDS projectile's penetration into the TNO-array. The values of the relevant parameters, that have been used in the simulation runs, are listed below.

35 mm FAPDS projectile:

mass front part	11.79 g
mass frangible part	244.91 g
mass rear part	43.59 g
shape factor of the fragments/particles	$0.004288 \text{ m}^2 / \text{kg}^{2/3}$
impact velocity	1400 m/s
impact angle	0 NATO
rifling twist of the gun	6°
number of particles into which a fragment breaks up (N_0)	$10 \leq N_0 \leq 100$
scattering angle for the individual fragments (α_i)	2°

The values of the last two parameters are not identical to the experimentally obtained values, but they proved to give better overall results. Explanations to justify these values are presented in this chapter.

Target damage

Figure 3 shows the damage caused by the fragments to the plates of the TNO-array as calculated with the FAPDS simulation program. This figure clearly demonstrates that synergism is not included in the simulation model, otherwise several big holes surrounded by zones of indents and cracks would be visible in the target plates.

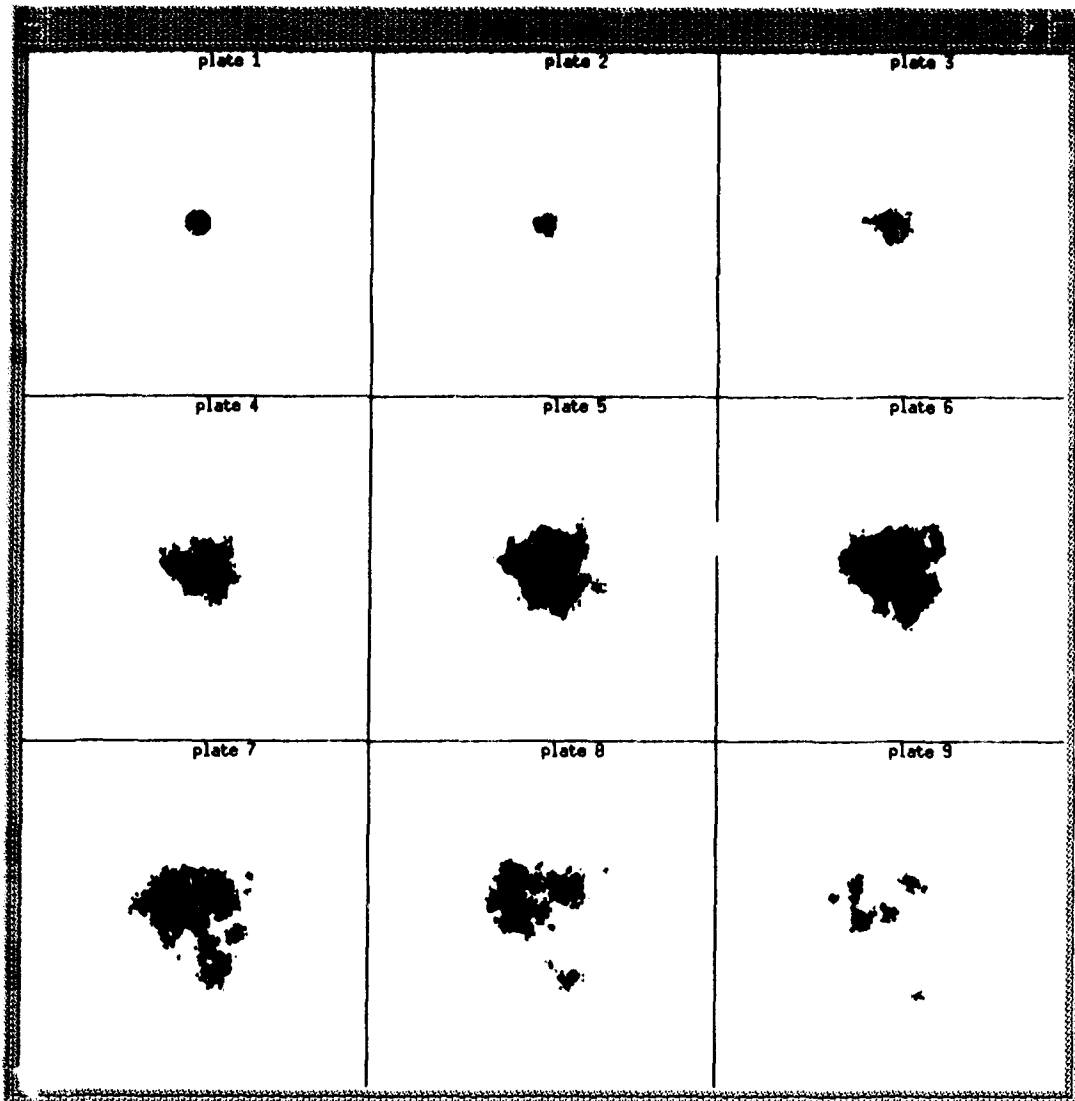


Figure 3 The damage caused to the plates of the TNO-array by a 35 mm FAPDS projectile (the holes and the non-perforating impacts are shown)

From the experiments it was deduced that the perforation pattern in a plate can be typically described by three damage areas [1]; a perforated zone, a zone which surrounds the perforated one and the non-perforating impacts, and a zone which encompasses all outward running cracks (Figure 4A). The hole diameter is defined as a characteristic dimension for the perforated zone, and it is determined by idealizing the perforated zone to a circle with an area equal to the measured hole area.

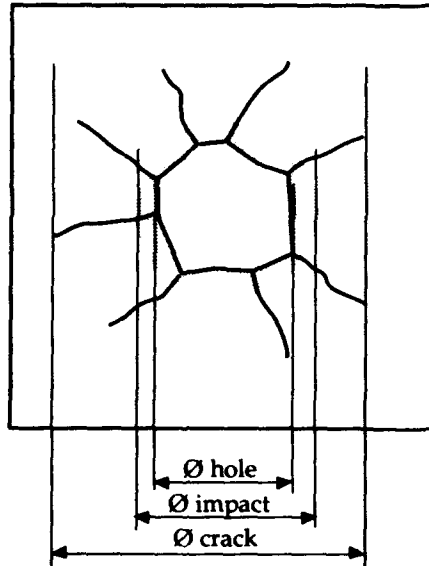


Figure 4A Definition of characteristic diameters (experiments)

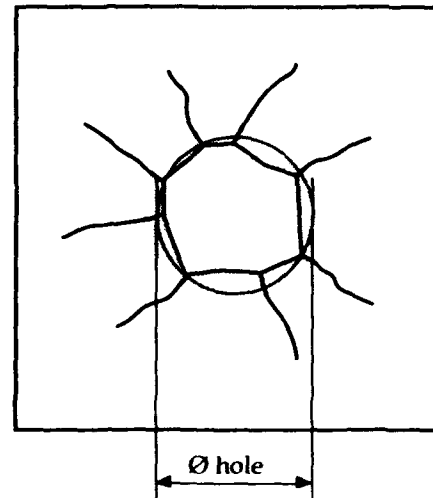


Figure 4B Definition of characteristic diameters (according to simulations)

In Figure 5, the hole diameters as measured in the TNO-array and as calculated by the FAPDS simulation program are shown. The hole diameter according to the simulations is defined as the diameter of the smallest circle which encompasses *all* holes in the target plate (Figure 4B). As a result, the hole diameters according to the simulations will be larger than the measured ones. By defining the hole diameter in such a way, the synergistic effect has been introduced in the evaluation of the simulation results. The hole diameter is an estimate of the hole area that would be measured in real targets.

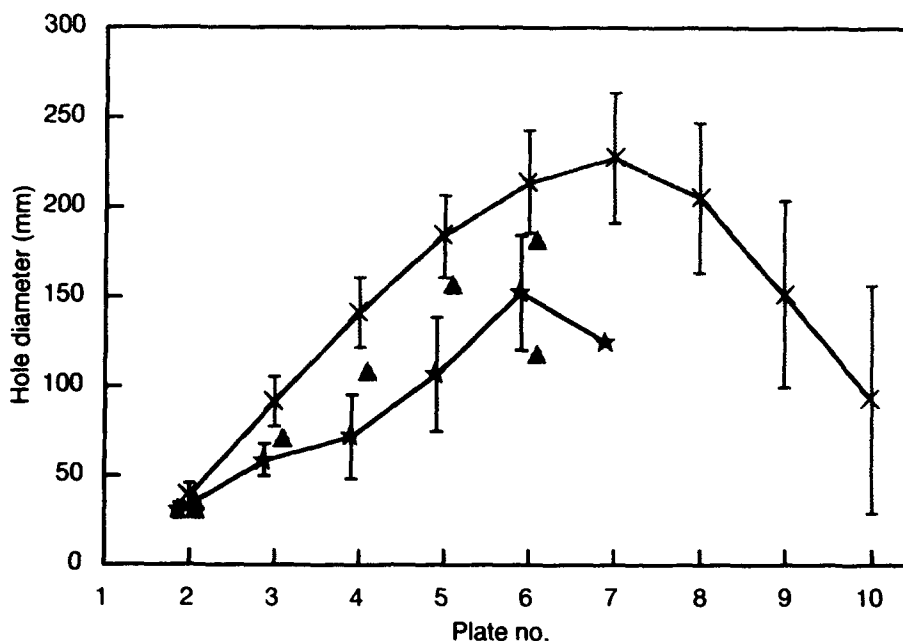


Figure 5 Experimental and theoretical hole diameters of the TNO-array
(★ experiments, ▲ experiments in which the hole diameters were similarly defined as in the simulations, × simulations)

The definition of the hole diameter as applied in the simulation results has also been applied to the experimental results. An estimate of this hole diameter was made by measuring the impact pattern in the fragment catcher, which was placed behind the last plate of the TNO-array. The results are also shown in Figure 5. Although these values tend to be greater than the originally measured ones, they still do not match the simulation results. However, one has to keep in mind that only an estimate could be presented, because the hole diameter was measured from the impact pattern in the fragment catcher in stead of the real target plates. Moreover, the impact patterns we used only showed the positions of the craters with a volume larger than 0.5 ml [2]. In the simulations all holes were taken into account, no matter how small they were.

The experiments showed that the hole diameters increase linearly until the sixth plate of the TNO-array after which a decrease sets in. The decrease is only indicative as it is based on one shot. The simulation shows an increase until the seventh plate after which the hole diameters decrease. The simulation results have also been compared to the results of experiments performed by Rheinmetall and BWB against target arrays like the TNO-array [8]. In general, the tendencies

predicted by the simulations are in agreement with the experimental results obtained by TNO, BWB and Rheinmetall. The maximum penetration capacity (i.e. the number of the last plate that was perforated) can be predicted well. Both the experiments and the simulations proved that up to ten or eleven plates of the target arrays can be perforated.

Mass distribution

Radiographs were used to measure the fragment masses after a specific target plate. The total mass of break-up material and the Mott parameter were calculated from these fragment masses. The relative mass of break-up material is defined as the total mass relative to the original mass of the projectile's frangible part, and is shown in Figure 6.

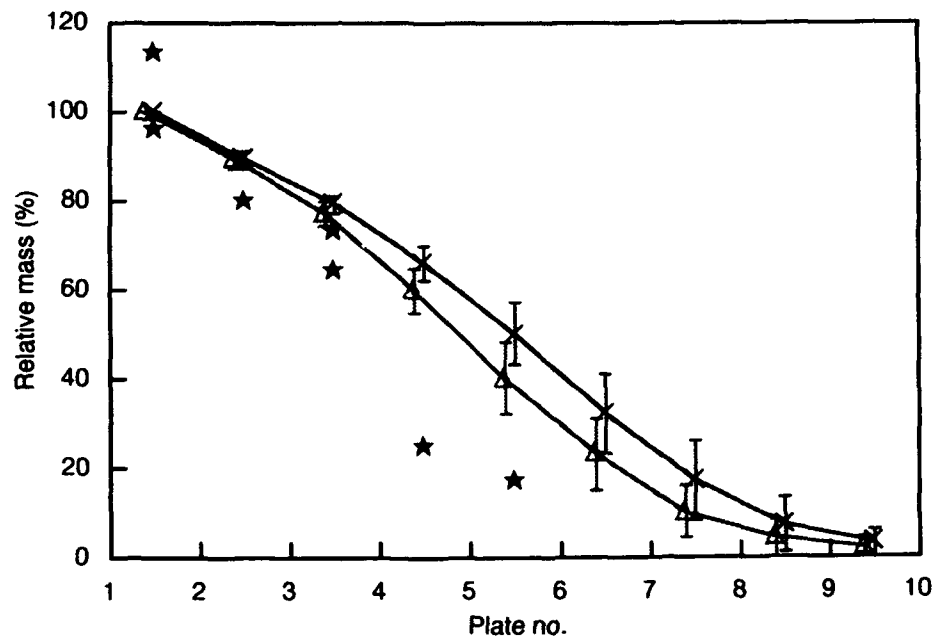


Figure 6 Experimental and theoretical relative mass of break-up material within the TNO-array (★ experiments, × simulations, Δ simulations in which only fragments heavier than 0.01 g were taken into account)

The simulation results underestimate the experimental results. The experiments indicated a mass loss of 20 percent at each target plate, the simulations a mass loss of 12 to 15 percent. The lost mass represents the fragments that were stopped by the target plates. However, in the experiments

the lost mass also represents the fragments that were too small to measure (< 0.01 g). An adapted theoretical relative mass is shown in Figure 6, which represents only the fragments heavier than 0.01 g. Although the results tend to be better this way, there still remains a gap between the experimental and theoretical results. Two reasons might justify this gap. Firstly, a limited number of experiments was performed, and the measurement of the fragment masses is not quite accurate (note the relative mass of 113 %). Secondly, the simulation results can be tuned by decreasing the number of particles into which a fragment breaks up (N_0). This way the simulation results can be improved with regard to the relative mass, but the agreement with other parameters will become worse. We have chosen the number of particles into which a fragment breaks up in such way, that the maximum penetration capacity of the fragment beam according to the simulation results agrees with the experimentally found maximum penetration capacity.

The mean fragment mass was determined from the experimental results through the determination of the Mott parameter. If the fragment mass distribution can be approximated by a Mott distribution, the mean fragment mass is equal to two times the Mott parameter. Figure 7 shows the Mott parameter.

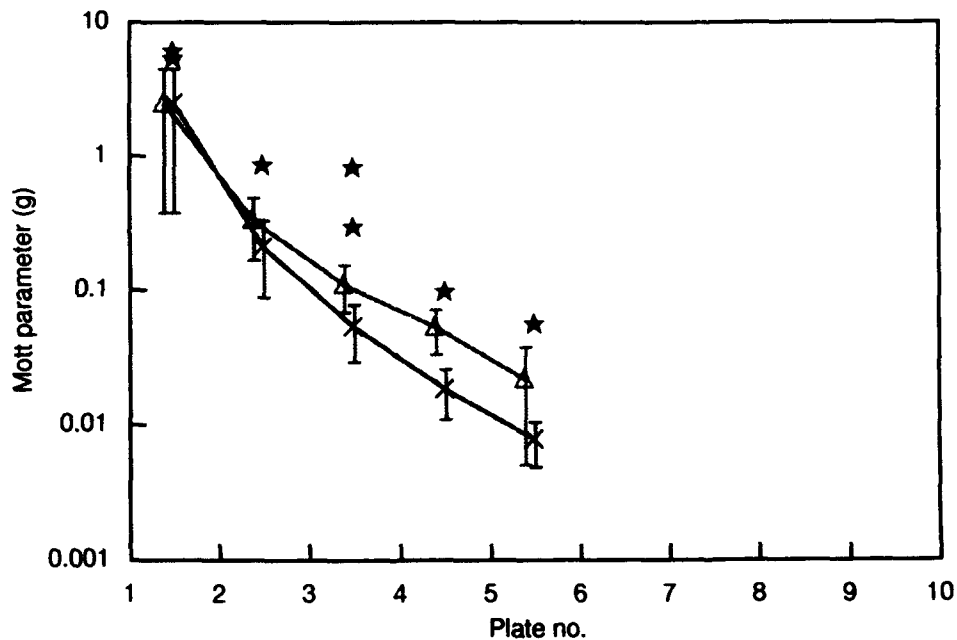


Figure 7 Experimental and theoretical values of the Mott parameter versus plate number of the TNO-array (★ experiments, × simulations, Δ simulations in which only fragments heavier than 0.1 g were taken into account)

The same reasoning held at the discussion of the relative mass holds for the discussion of the Mott parameter. The deviation between the experimental and theoretical Mott parameters depends on the accuracy of the measurements, and on the number of particles into which a fragment breaks up. To demonstrate the influence of the accuracy of the measurements, another estimate of the Mott parameter is shown in Figure 7. Based on the same fragment mass distribution, we have increased the lower limit from 0.01 g to 0.1 g. The resulting Mott parameter increases dramatically, especially after the fourth target plate where lots of tiny fragments are present.

Spatial distribution

In Figure 8, the experimental and theoretical cone angles are shown. The cone angle is defined as the aperture angle of the cone which encloses all fragments of the fragment beam.

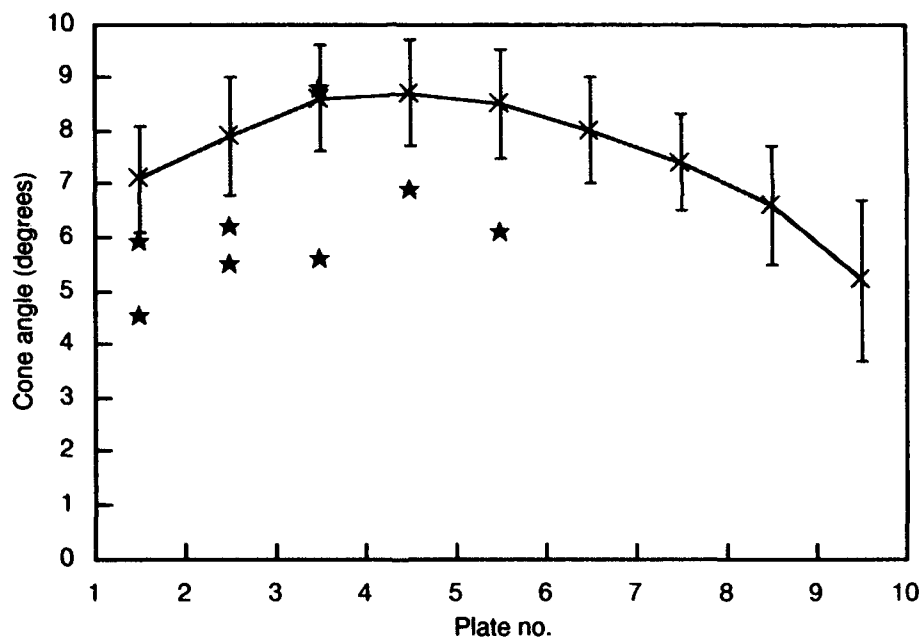


Figure 8 Experimental and theoretical cone angles within the TNO-array
(★ experiments, X simulations)

Experiments indicated that the cone angle remains almost constant in the target arrays. Moreover, the cone angle seemed to be independent of the target array composition. The simulation results are in good agreement with the experimental ones, although the simulations predict larger values. The measured cone angles can be underestimated, since they were measured from radiographs.

These radiographs do not show fragments smaller than 0.01 g. If the fragments smaller than 0.01 g are left out, the theoretical cone angles will become about 10 percent smaller.

The impact patterns in the fragment catchers located behind the target arrays were used to determine the number of craters, or properly speaking the number of fragments and their spatial distribution. The craters were divided into two groups; the large craters with volumes larger than 0.5 ml, and the small craters with volumes smaller than 0.5 ml. An equivalent distinction has been applied to the simulation results; large fragments with a mass larger than 1.786 g, and small fragments with a mass smaller than 1.786 g. The relation between crater volume and fragment mass was derived in [2]. The total number of small and large fragments is presented in Figure 9.

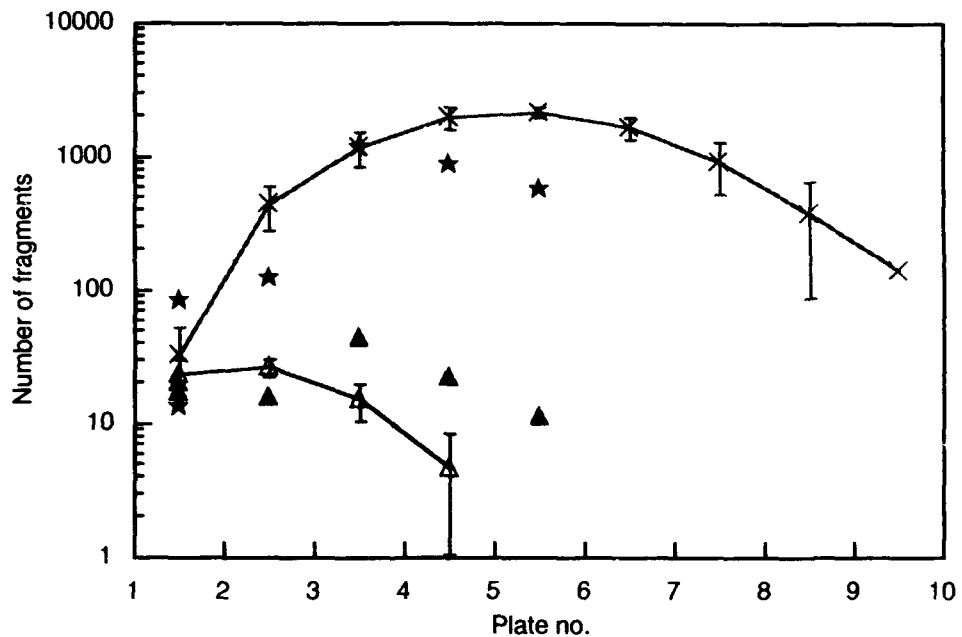


Figure 9 Experimental and theoretical total number of small and large fragments within the TNO-array (small fragments: ★ experiments, × simulations || large fragments: ▲ experiments, △ simulations)

The number of small and large fragments is in the same order of magnitude for the experimental and simulation results. At the beginning of the target array, the numbers agree well; moving further in the target plate array, the differences increase which might be explained by the large amount of small fragments. The smaller the fragments, the worse the determination of its number.

Kinetic energy

The crater volumes were also used to determine the kinetic energy of the fragment beam. It is assumed that the volume is proportional to the kinetic energy. The total crater volume and the theoretical relative total energy are shown in Figure 10. In contrast to the other results, the crater volume and the kinetic energy include the contribution of the nose and rear part of the FAPDS projectile.

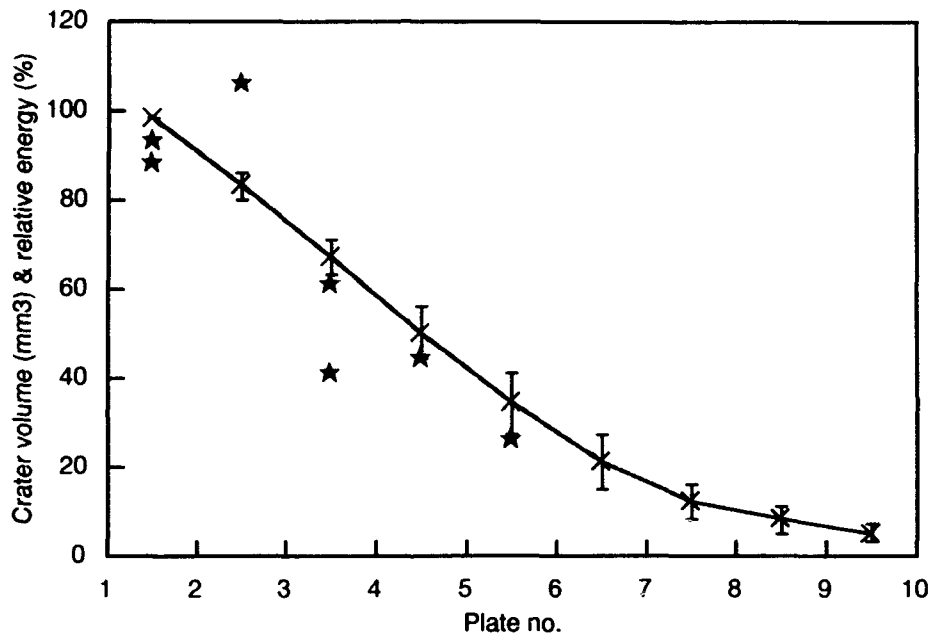


Figure 10 Total crater volume versus plate number as measured by the experiments (★), and relative kinetic energy of the beam within the TNO-array as calculated by the simulations (×)

Although the dimensions of the series in Figure 10 are different, the tendencies are in perfect harmony. The decrease in energy is about 16 to 18 % per target plate. Therefore, it is obvious that the maximum penetration capacity is consistent for the experiments and the simulations.

An essential distinction between the experimental and the simulation results exists, however. The decrease in energy is equal to the decrease of the measured fragment mass per target plate. Meaning, the velocity decay of the fragments is negligible according to the experiments. According to the simulation results, the decrease in energy is larger than the decrease in fragment mass, and as a result the velocity decay of the fragments is not negligible.

4.2 Influence of target composition and rifling twist

Next to the experiments with TNO-arrays, modified TNO-arrays were used as well. We will discuss the results of experiments and simulations in which one of the aluminium plates of the TNO-array was replaced by a 4 mm steel 52 plate. The steel plates were located at position two and six respectively. The damage to the modified arrays is shown in Figure 11.

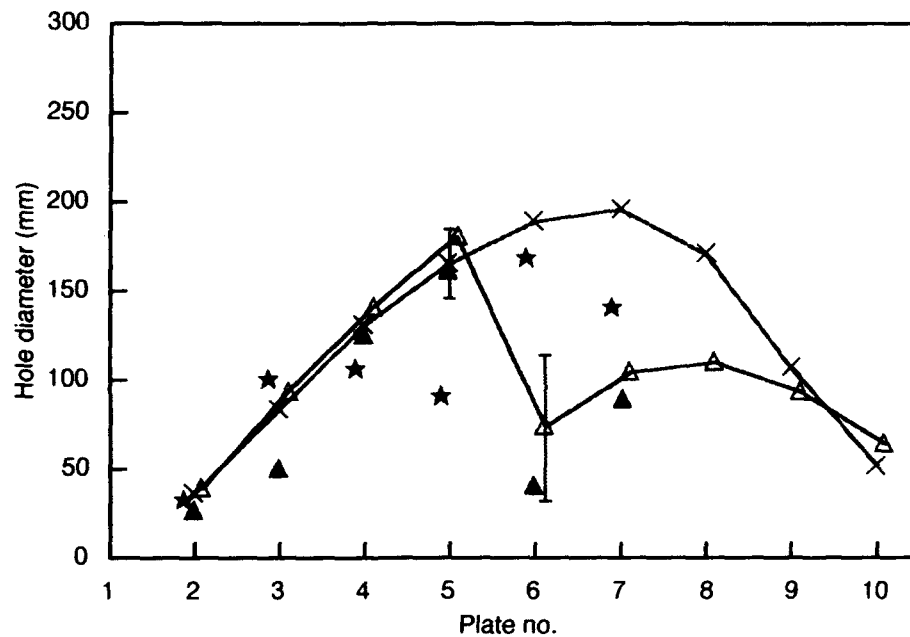


Figure 11 Experimental and theoretical hole diameters of the TNO-array with steel plates at position 2 and 6 (steel plate at position 2: ★ experiments, × simulations || steel plate at position 6: ▲ experiments, △ simulations)

The experimental and simulation results are in good agreement. Replacement of the aluminium plate by a steel plate at position 2 has hardly any influence on the damage pattern. Replacement of the plate at position 6 has a distinct influence; the hole diameter of the sixth plate decreases radically, and the subsequent hole diameters decrease too. This effect can be explained by the so-called overload concept [2]; at the beginning of the array the fragment beam has enough kinetic energy to perforate any target plate, further down the fragment beam does not have such "overload" capacity any more.

The influence of the rifling twist on the simulation results is clearly shown in Figure 12. By doubling the rifling twist from 6 to 12 degrees, a similar increase in cone angle can be noticed. A plausible explanation has been presented in the discussion of the fragmentation model. Experiments have demonstrated the same effect [6].

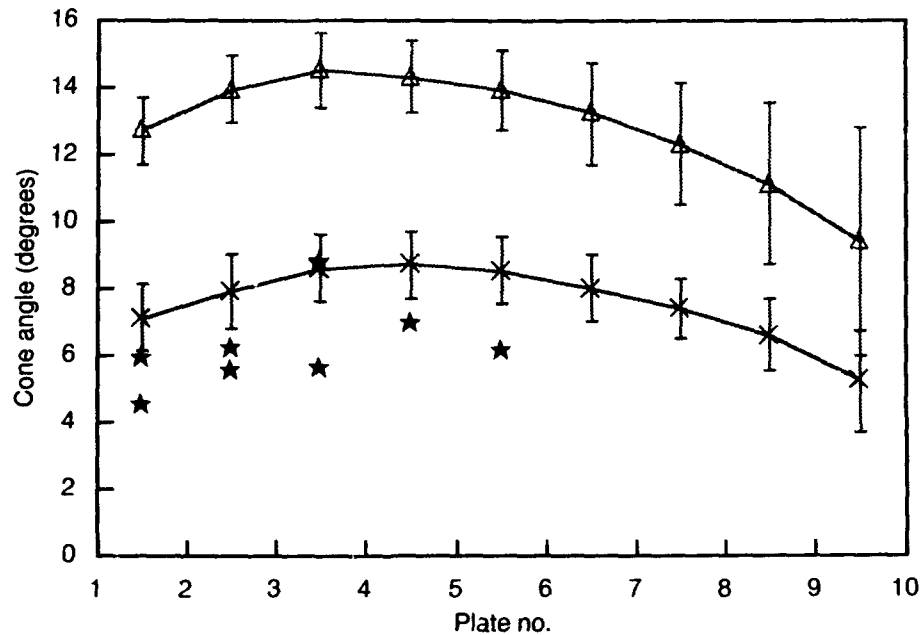


Figure 12 Experimental and theoretical cone angles within the TNO-array (★ experiments with RT=6°, × simulations with RT=6°, Δ simulations with RT=12°)

4.3 Influence of parameters of the simulation model on the results

The simulation model discussed so far has been optimised to produce results, that are consistent with the experimental results. In this section, the influence of mass distribution and scattering angle on the simulation results is discussed. This way, we hope to demonstrate the urgent need for more experimental data relevant to the fragmentation process.

The influence of the maximum number of particles into which a fragment breaks up (N_0) is shown in Figure 13 (using a Mott distribution in both situations).

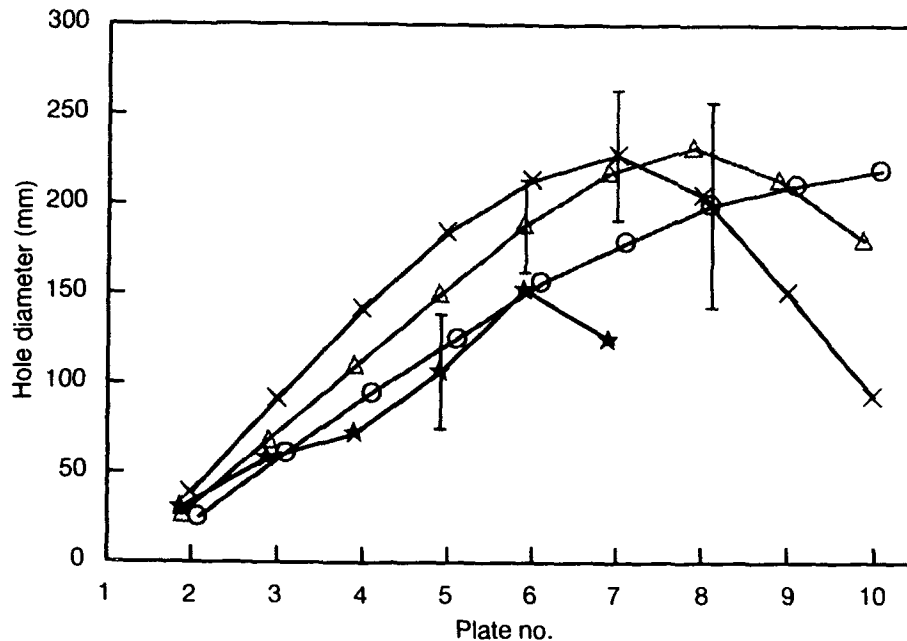


Figure 13 Experimental and theoretical hole diameters of the TNO-array (★ experiments, × Mott distribution and $10 \leq N_0 \leq 100$, △ Mott distribution and $10 \leq N_0 \leq 20$, ○ random distribution and $10 \leq N_0 \leq 100$; N_0 is the number of particles into which a fragment breaks up)

As stated before, experiments indicated that the maximum number of particles into which a fragment breaks up should be about 20 [2]. The simulation model gives better overall results when the maximum number of particles is increased to 100. By increasing the maximum number of particles, the average mass of the particles is being reduced, and as a result, the penetration capacity of the fragment beam too. The fragment beam becomes wider, which results in larger hole diameters as shown in Figure 13.

The maximum number of 100 (or even more) as indicated by the simulation results is reasonable. The experimental values were obtained by radiographs. The particles on these radiographs are hard to distinguish. Moreover, particles less than 0.01 g are not shown on these radiographs. Therefore, the experimental values are underestimated.

The influence of the type of mass distribution is shown in Figure 13 as well. A Mott distribution is compared to a random distribution (using 100 as the maximum number of particles into which a fragment breaks up in both situations). The random distribution consists of a few larger particles and lots of tiny particles. As a result, even after the perforation of several plates, a few heavy particles will remain. The penetration capacity is, amongst other things, related to the existence of

these heavy particles. A Mott distribution gives a somewhat more uniform mass distribution with regard to the random distribution. Therefore, the penetration capacity will be less and the fragment beam wider whenever a Mott distribution instead of a random distribution is used.

As mentioned above, an increase in the number of particles into which a fragment breaks up (N_0) results in a wider fragment beam. Another possibility to control the fragment beam width is to change the scattering angle for the individual fragments (α_i) as shown in Figure 14.

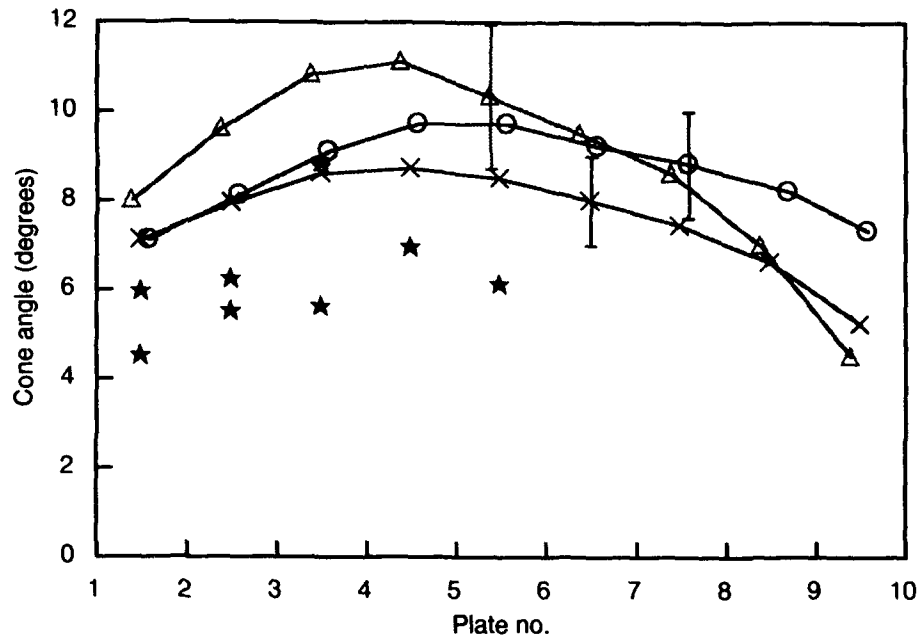


Figure 14 Experimental and theoretical cone angles within the TNO-array (★ experiments, × Mott distribution and $10 \leq N_0 \leq 100$ and $\alpha_i=2^\circ$, △ Mott distribution and $10 \leq N_0 \leq 100$ and $\alpha_i=3^\circ$, ○ Mott distribution and $10 \leq N_0 \leq 20$ and $\alpha_i=3^\circ$)

The scattering angle for the individual fragments does not only affect the fragment beam width, but also the penetration capacity of the beam. The scattering angle of 2 degrees in combination with the maximum number of particles of 100 proved to give the best overall results. In Figure 14 the simulation results using the original experimental values are shown too. For this particular situation the fragment beam width is not that bad, but the maximum penetration capacity is far out of line.

Concluding remarks

During the development of the simulation model, we tried to match the simulation results to the experimental ones. Since dependencies are incorporated, this matching process is quite complicated. For example, if we decrease the scattering angle for the individual fragments, the cone angle decreases, but at the same time the penetration capacity of the fragment beam increases. So, on the one hand we achieve better results for the cone angle, but on the other hand worse results for the hole diameters. From all parameters which could be compared, the penetration capacity of the fragment beam has been marked as the most important parameter.

The simulation model probably can be improved, if more information on the fragmentation process of the individual fragments is available. Planned experiments with frangible FSPs hopefully will provide this information.

5 THE IMPLEMENTATION OF THE FAPDS SIMULATION MODEL IN A VULNERABILITY ASSESSMENT CODE

Because of the encouraging simulation results, it was decided to implement the FAPDS simulation model in a vulnerability assessment code. The simulation model proves that the break-up mechanism of the individual fragments and the effect of parasitism can be implemented in a straightforward way in a shot line based vulnerability code. However, the final implementation gives rise to some as yet unresolved problems.

The major problem is to find a way to deal with synergistic effects. In the TNO-array, large holes were created, and cracks were formed. The target plates were often bent and petals were formed. Little is known about these phenomena. Models to describe these mechanisms in order to implement them in a terminal ballistics model still have to be developed.

Another major problem is the difference between real targets and the simple target plate arrays. Live firings proved that for instance electronic compartments and fuel tanks have a significant influence on the damage pattern. Replacing the electronic compartments and fuel tanks with simple boxes is not sufficient to obtain reliable simulation results.

The FAPDS simulation model is based on a shot line method; for every fragment/particle a shot line is created. Along these shot lines calculations are performed to determine the extent of penetration. Using a simple target array with 10 plates will result in about 100,000 shot lines to be evaluated. Because of the Monte Carlo character of the simulation model, several simulation runs (about 50) have to be performed to obtain statistically significant results.

One possible solution to reduce the number of shot lines to be evaluated is to define thresholds. For instance, the minimum mass necessary to perforate the weakest part of the target could be calculated. Then the shot lines for fragments with masses less than the minimum mass do not have to be evaluated in a simulation run. This method has already been applied to the results as presented in Chapter 4. We have defined a threshold of 0.001 g, which represents the minimum mass necessary to perforate the 2 mm aluminium plates of the TNO-array.

Another approach which could be considered is the fragment density method. With this method, individual fragments are no longer traced through the target, but they are combined into one single beam. The beam has to be characterized by at least two parameters, the beam width and the penetration capacity of the beam. Effects like breaking up, parasitism, and synergism do not have to be described in detail for the individual fragments. Using this approach, one has to tackle a new problem, how to determine the characteristic parameters of the beam. A preliminary study [9] indicated that the influence of the beam width on effectiveness computations cannot be neglected. The influence depends on the component dimensions of the target model used in the effectiveness calculations.

Both methods (shot line and beam) have advantages and disadvantages. At the moment, we are examining which method can be applied best for vulnerability assessment studies. Probably a mixture of both methods, in which a limited number of shot lines will be evaluated, will be chosen. The shot lines represent the fragment beam. Penetration equations will be applied for every shot line (just like the THOR equations). Afterwards, the penetration data of the individual shot lines will be combined to obtain the final damage inflicted upon the target.

6 CONCLUSIONS

A semi-empirical terminal ballistics model for FAPDS munition has been developed. This model is based on relatively simple descriptions for the penetration and fragmentation processes. The effect of parasitism is included. The effect of synergism has been included in the aggregation of results.

Comparison of simulation results with experiments for 35 mm FAPDS munition against target plate arrays is satisfactory. Two major characteristics, i.e. the maximum penetration capacity and the fragment beam width, can be calculated accurately with aid of the simulation program. The influence of the target array composition and the rifling twist of the gun on the simulation results can be predicted well.

Further improvement of the simulation results is possible, when more information on the details of the fragmentation process becomes available. It is expected that experiments with frangible FSPs will provide this information.

One has to keep in mind that the results presented are valid for the 35 mm FAPDS projectile as described in Chapter 2 only. Other kinds of FAPDS projectiles might require new or adapted models to describe the fragmentation process.

Although the problems affiliated with the implementation of the terminal ballistics model in a vulnerability code have not been resolved yet, it is expected that these problems will be solved in the near future.

7 AUTHENTICATION



Ir. T.L.J. Keij
(project leader, author)

8 REFERENCES

- 1 Gillis, M.P.W.
An experimental analysis of the terminal behaviour of 35 mm FAPDS munition.
Report PML 1988-21, TNO Prins Maurits Laboratory (CONFIDENTIAL)
- 2 Gillis, M.P.W., Reith, J.M.
An experimental analysis of the terminal behaviour of 35 mm FAPDS munition.
Second program.
Report PML 1990-78, TNO Prins Maurits Laboratory (CONFIDENTIAL)
- 3 Gillis, M.P.W.
Theoretical analysis of some aspects of 35 mm FAPDS munitions' terminal ballistic behaviour.
Report PML 1991-6, TNO Prins Maurits Laboratory (CONFIDENTIAL)
- 4 J.L.M.J. van Bree, M.P.W. Gillis
Frangible Armour Penetrator, An Experimental Analysis and Preliminary Analytical
Description of its Performance in Multiple Plate Arrays.
Proceedings 12th International Symposium on Ballistics, San Antonio, U.S.A., 1990.
- 5 A.J. Baart, T.L.J. Keij
FAPDS Simulation; The First Implementation of a Frangible Armour Piercing Ammunition
Model.
Report PML 1992-6, TNO Prins Maurits Laboratory
- 6 Gillis, M.P.W.
Evaluation of experiments with 35 mm FAPDS munition performed by BWB (West
Germany).
Report PML 1989-5, TNO Prins Maurits Laboratory (CONFIDENTIAL)
- 7 Anonymous
The Resistance of Various Metallic Materials to Perforation by Steel Fragments.
Project Thor Report 47, 1961, Ballistic Research Laboratory

8 Bisping

Zünder- und sprengstoffloses Splittergeschoss

Bericht Nr. 150-006-82, Rheinmetall (VS-Vertraulich)

9 E. van Meerten

Preliminary research concerning the implementation of 35 mm FAPDS in the TARVAC vulnerability code.

Report no. PML 1992-2, TNO Prins Maurits Laboratory

9 LIST OF SYMBOLS

A	average presented area	m ²
C	projectile calibre	mm
D	projectile diameter	mm
L	line-of-sight thickness	mm
m	fragment mass	g
\bar{m}	mean fragment mass	g
m _{in}	fragment mass before penetration of a target	g
m _{out}	residual fragment mass after penetration of a target	g
N(m)	cumulative number of fragments with mass $\geq m$	
N ₀	maximum number of particles into which a fragment breaks up	
r	hole radius	mm
RT	rifling twist	degrees
S	shape factor	m ² / kg ^{2/3}
t	target thickness	mm
v	fragment velocity	m/s
v ₀	muzzle velocity	m/s
v _{in}	fragment velocity before penetration of a target	m/s
v _{out}	residual fragment velocity after penetration of a target	m/s
v _{t max}	maximum tangential fragment velocity	m/s
α	scattering angle	degrees
α_{max}	maximum scattering angle	degrees
θ	angle between the surface normal and the fragment trajectory	degrees
ω	spin rate	1/s
Δt	perforation time	s

ANNEX A THE MODIFIED THOR EQUATIONS

The THOR equations probably are the most familiar equations to calculate the residual mass and velocity of fragments after penetration of a target plate. The THOR equations were derived experimentally from ballistic tests [7] for a large number of combinations of compact steel fragments, target materials and set-ups.

The THOR equations are valid for homogeneous "infinite" target plates. As explained in Chapter 3, this specific condition is not always valid for FAPDS munition. Situations occur in which fragments encounter holes in the target plates. Depending on the dimensions of the fragments and of the holes, some fragments can fly through the holes without any interaction with the target plate (parasitism). Other fragments, that are larger than the holes, will interact with the target plate, and as a result will break up. Besides, the energy of the fragments will be reduced, and the holes in the target plate will be enlarged. To calculate the residual mass and velocity of these semi-parasitic fragments, we have derived the so-called modified THOR equations. The derivation of these equations is discussed below.

The THOR equations are the basics for the modified THOR equations. Therefore, we will summarize some part of Chapter 3 in which the THOR equations were discussed.

Consider the configuration shown in Figure A.1.

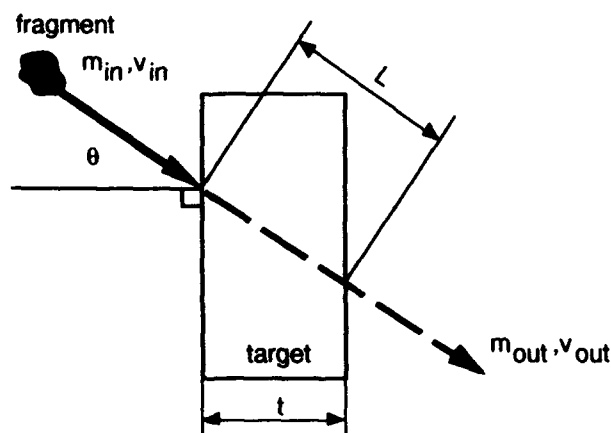


Figure A.1 A fragment penetrating a target

A fragment with mass m_{in} and velocity v_{in} hits the target. The angle between the velocity vector of the fragment and the normal of the target surface is defined as θ . During the penetration, the

velocity of the fragment as well as its mass reduces. If the fragment strikes the target with sufficient energy, it will perforate the target. The residual mass m_{out} and velocity v_{out} can be calculated with aid of the following THOR equations:

$$v_{out} = v_{in} - 10^{C1} * (t * A)^{C2} * m_{in}^{C3} * \left(\frac{1}{\cos \theta} \right)^{C4} * v_{in}^{C5} \quad (A.1)$$

$$m_{out} = m_{in} - 10^{K1} * (t * A)^{K2} * m_{in}^{K3} * \left(\frac{1}{\cos \theta} \right)^{K4} * v_{in}^{K5} \quad (A.2)$$

where $C1..C5$ and $K1..K5$ are material constants

t = target thickness

A is the average presented area of the fragment calculated from the shape factor S and the mass m_{in} :

$$A = S * m_{in}^{2/3} \quad (A.3)$$

If the residual mass or velocity is less than or equal to zero, the fragment is not capable of perforating the target.

For the derivation of the modified THOR equations, we use the situation as shown in Figure A.2.

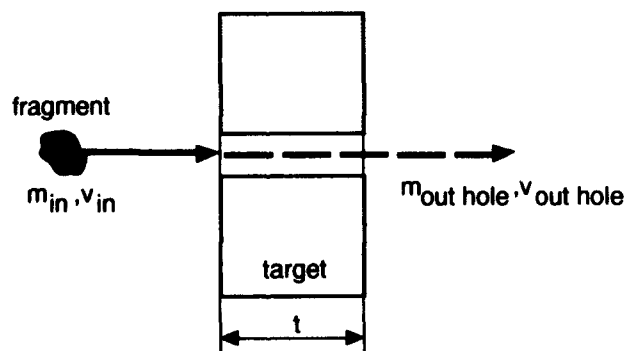


Figure A.2 A fragment flying through a hole in the target

A fragment with mass m_{in} and velocity v_{in} hits the target at the location where a hole is present. The area of the hole is A_{hole} (frontal area). The presented area of the fragment is defined by equation A.3.

We will only consider the situations of normal impact, which are of most interest for FAPDS munition (the striking angles are small, up to about 3°). As a result, the modified THOR equations will be valid for normal impacts and for small impact angles. We assume that the centre of mass of the fragment flies through the centre of the hole. This way, we neglect troublesome phenomena, such as tumbling of the fragment which might occur if the fragment strikes the edge of the hole. Finally, we assume that the cross section of the hole is equal along the axis of the hole.

Regarding the situation shown in Figure A.2, two possibilities arise:

- 1 The fragment is smaller than the hole.

$$A < A_{hole} \quad (A.4)$$

or

- 2 The fragment is larger than the hole, or has an equal dimension.

$$A \geq A_{hole} \quad (A.5)$$

The first possibility is quite simple to deal with; the fragment flies through the hole without loss of energy. Meaning:

$$m_{out\ hole} = m_{in}, \text{ and } v_{out\ hole} = v_{in} \quad (A.6)$$

where $m_{out\ hole}$ and $v_{out\ hole}$ represent the residual mass and velocity of a fragment that went through a hole in the target plate

The second possibility is far more complex. The energy of the fragment will be reduced, because the fragment has to penetrate the target. The residual mass and velocity of the fragment will be larger with regard to the situation in which no hole is present in the target plate. As a result, the existing hole will be enlarged.

Consider the situation in which no hole is present in the target plate. The energy of the fragment before and after penetration is defined by equations A.7 and A.8.

$$E_{in} = \frac{1}{2} * m_{in} * v_{in}^2 \quad (A.7)$$

$$E_{out} = \frac{1}{2} * m_{out} * v_{out}^2 \quad (A.8)$$

The energy E_{perf} i.e. the energy needed to perforate the target plate, is defined as the difference.

$$E_{perf} = E_{in} - E_{out} \quad (A.9)$$

The derivation of the modified THOR equations is based on energy conservation laws. What will be done is to add the minimum amount of energy needed to perforate the target plate (and create a hole with area A_{hole}) to the residual energy of the fragment if no hole was present in the target plate (equation A.8). From the resulting residual energy the residual mass $m_{out\ hole}$ and velocity $v_{out\ hole}$ can be calculated.

The minimum energy needed to create a hole (with frontal area A_{hole} in a target plate of thickness t) results from equation A.10.

$$\frac{\partial E_{perf}(m_{in}, v_{in})}{\partial v_{in} \partial m_{in}} = \frac{\partial (E_{in} - E_{out})}{\partial v_{in} \partial m_{in}} = 0 \quad (A.10)$$

The hole size is chosen to be equal to the presented area of the fragment, that created the hole. As a result, m_{in} is set by equation A.11.

$$m_{in} = \left(\frac{A_{hole}}{S} \right)^{3/2} \quad (A.11)$$

Equation A.10 can be solved by use of equation A.11 and the THOR equations. This is a rather complicated problem, while the THOR equations are interrelated, and can only be used if m_{out} and v_{out} are greater or equal to zero.

Therefore, another approach has been selected in which the residual energy E_{out} has been set to zero. Now, the THOR equations can be used to calculate the value of v_{in} corresponding to the minimum perforation energy. This value of v_{in} will be referred to as v_p . The value of m_{in} corresponding to the minimum perforation energy will be referred to as m_p . The minimum perforation energy $E_{perf\ min}$ can be calculated with aid of equation A.12.

$$E_{perf\ min} = \frac{1}{2} * m_p * v_p^2 \quad (A.12)$$

where

$$m_p = \left(\frac{A_{hole}}{S} \right)^{3/2} \quad (A.13)$$

and $v_p =$ minimum of

$$\left(10^{C1} * (t * A_{hole})^{C2} * m_p^{C3} * \left(\frac{1}{\cos \theta} \right)^{C4} \right)^{\frac{1}{1-C5}}$$

and

$$\left(10^{-K1} * (t * A_{hole})^{-K2} * m_p^{1-K3} * \left(\frac{1}{\cos \theta} \right)^{-K4} \right)^{\frac{1}{K5}} \quad (A.14)$$

As said before, the minimum perforation energy ($E_{perf\ min}$) is to be added to the residual energy of the fragment (E_{out}) if no hole was present in the target plate. The sum of those energies is the residual energy of the fragment ($E_{out\ hole}$), that penetrated the target plate with the hole.

Once again, we have to distinct the following three situations:

- 1 The energy of the fragment is sufficient to penetrate even an equivalent target plate without any hole.

$$E_{out} > 0 \quad (A.15)$$

- 2 The energy of the fragment is sufficient to penetrate the target plate while a hole in the target plate is present.

$$E_{out} \leq 0$$

and

$$E_{out\ hole} (= E_{out} + E_{perf\ min}) > 0 \quad (A.16)$$

- 3 The energy of the fragment is not sufficient to penetrate the target plate, even if a hole is present in the target plate.

$$E_{out} \leq 0$$

and

$$E_{out\ hole} (= E_{out} + E_{perf\ min}) \leq 0 \quad (A.17)$$

Negative energies have been used to indicate that the fragment is not capable of perforating the target plate.

For each of the three situations mentioned above, the parameters $m_{out\ hole}$ and $v_{out\ hole}$ can be derived from equation A.18.

$$E_{out\ hole} = \frac{1}{2} * m_{out\ hole} * v_{out\ hole}^2 = E_{out} + E_{perf\ min} \quad (A.18)$$

However, this is only one equation, while we have to determine two parameters. We use the THOR equations to solve this problem. As shown by these equations, the residual mass and velocity of a fragment is determined by $(t^*A)^{K2}$ and $(t^*A)^{C2}$ respectively. The id. (t^*A) is the volume of target material, that has to be removed from the target plate during penetration. In other words, the id. (t^*A) represents some kind of ballistic resistance, which has to be broken. Equation A.18 can be solved using this information. The penetration of a target plate with a hole is compared to the penetration of a target plate of less ballistic resistance. The ballistic resistance, in particular the id. (t^*A) , will be referred to as BRC (Ballistic Resistance Coefficient).

The following equations can be derived from the THOR equations at given m_{in} , v_{in} and θ :

$$m_{out} \sim (BRC)^{K2} \quad (A.19)$$

$$v_{out} \sim (BRC)^{C2} \quad (A.20)$$

As a result:

$$E_{out} \sim (BRC)^{K2+2^*C2} \quad (A.21)$$

Comparing the penetration of a target plate with a hole to the penetration of a target plate of less ballistic resistance (BRC_{hole}), we arrive at the following equations:

$$m_{out\ hole} = \left(\frac{BRC_{hole}}{BRC}\right)^{K2} * m_{out} = \left(\frac{E_{out\ hole}}{E_{out}}\right)^{\frac{K2}{K2+2^*C2}} * m_{out} \quad (A.22)$$

$$v_{out\ hole} = \left(\frac{BRC_{hole}}{BRC}\right)^{C2} * v_{out} = \left(\frac{E_{out\ hole}}{E_{out}}\right)^{\frac{C2}{K2+2^*C2}} * v_{out} \quad (A.23)$$

where BRC = the ballistic resistance coefficient of the target plate without holes.

Equations A.22 and A.23 form the modified THOR equations. They provide the solution for situation no.1, which has been described earlier; the energy of the fragment is sufficient to penetrate an equivalent target plate even without any hole.

The solution of situation no. 2 (the energy of the fragment is sufficient to penetrate the target plate while a hole in the target plate is present) is not available yet. The modified THOR equations can not be used, because m_{out} and/or v_{out} are not valid ($m_{out} \leq 0$ and/or $v_{out} \leq 0$). In the FAPDS simulation model, this problem has been resolved by assuming that the hole in the target plate will be enlarged, but the residual energy of the fragment will be negligible.

The solution of situation no. 3 (the energy of the fragment is not sufficient to penetrate the target plate, even if a hole is present in the target plate) is simply given by equation A.24

$$m_{out\ hole} = 0, \text{ and } v_{out\ hole} = 0 \quad (A.24)$$

The explanation is obvious; the fragment is not capable of perforating the target plate. In the FAPDS simulation model, we assumed that the fragment will not enlarge the hole in the target plate.

Summary

The following assumptions have been made to derive the modified THOR equations:

- 1 Normal impact of the fragments on the target plate. However, the results may also be used for small impact angles.
- 2 Phenomena, such as tumbling of the fragment which might occur if the fragment strikes the edge of the hole, are neglected.
- 3 The cross section of the hole is equal along the axis of the hole.
- 4 The hole size is equal to the presented area of the fragment, that created the hole.
- 5 The penetration of a target plate with a hole can be compared to the penetration of a target plate of less ballistic resistance.

The following situations can be distinguished:

- I The fragment is smaller than the hole, meaning:

$$A < A_{hole}$$

Results:

$$m_{\text{out hole}} = m_{\text{in}}, \text{ and } v_{\text{out hole}} = v_{\text{in}}$$

II The fragment is larger than the hole, and the energy of the fragment is sufficient to penetrate an equivalent target plate even without any hole.

$$A \geq A_{\text{hole}}$$

and

$$E_{\text{out}} > 0$$

Results:

$$m_{\text{out hole}} = \left(\frac{E_{\text{out}} + E_{\text{perf min}}}{E_{\text{out}}} \right)^{\frac{K2}{K2+2*C2}} * m_{\text{out}}$$

$$v_{\text{out hole}} = \left(\frac{E_{\text{out}} + E_{\text{perf min}}}{E_{\text{out}}} \right)^{\frac{C2}{K2+2*C2}} * v_{\text{out}}$$

where $E_{\text{perf min}} = \frac{1}{2} * \left(\frac{A_{\text{hole}}}{S} \right)^{3/2} * v_p^2$

and $v_p = \text{minimum of}$

$$\left(10C1 * (t * A_{\text{hole}})^{C2} * \left(\frac{A_{\text{hole}}}{S} \right)^{3/2} C3 * \left(\frac{1}{\cos \theta} \right)^{C4} \right)^{\frac{1}{1-C5}}$$

and

$$\left(10^{-K1} * (t * A_{\text{hole}})^{-K2} * \left(\frac{A_{\text{hole}}}{S} \right)^{3/2} (1-K3) * \left(\frac{1}{\cos \theta} \right)^{-K4} \right)^{\frac{1}{K5}}$$

III The fragment is larger than the hole and the energy of the fragment is sufficient to penetrate the target plate while a hole in the target plate is present.

$$A \geq A_{\text{hole}}$$

and

$$E_{\text{out}} \leq 0$$

and

$$E_{\text{out hole}} (= E_{\text{out}} + E_{\text{perf min}}) > 0$$

Results: Not known.

In the FAPDS simulation model, we have assumed:

$m_{\text{out hole}} = 0$, and $v_{\text{out hole}} = 0$, and the hole is enlarged

IV The fragment is larger than the hole, and the energy of the fragment is not sufficient to penetrate the target plate, even if a hole is present in the target plate.

$$A \geq A_{\text{hole}}$$

and

$$E_{\text{out}} \leq 0$$

and

$$E_{\text{out hole}} (= E_{\text{out}} + E_{\text{perf min}}) \leq 0$$

Results:

$$m_{\text{out hole}} = 0, \text{ and } v_{\text{out hole}} = 0$$

ANNEX B THE FAPDS SIMULATION COMPUTER PROGRAM

The FAPDS simulation computer program has been described in Chapter 3. The structure of the program is discussed in this Annex.

The FAPDS simulation computer program is built modularly, as illustrated in Figure B.1.

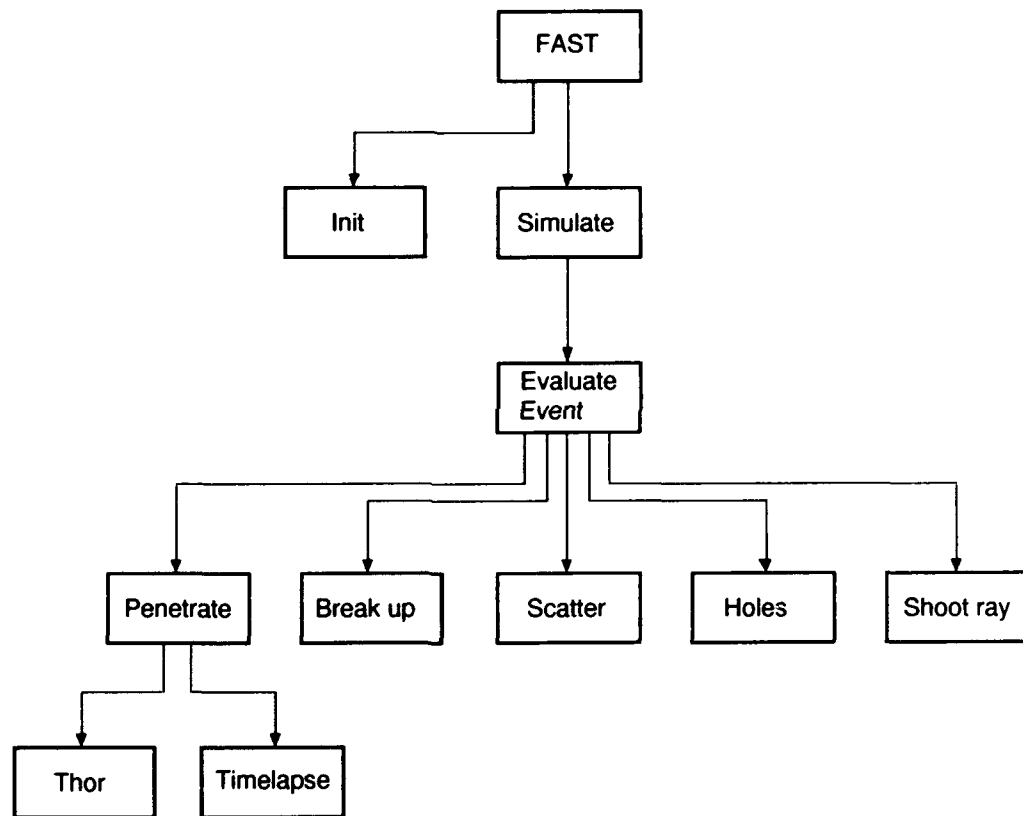


Figure B.1 Structure of FAPDS simulation computer program.

The main module entitled '*FAST*' uses the modules '*Init*' and '*Simulate*'. '*Simulate*' contains the simulation loop in which the '*Evaluate Event*' module, the key to the simulation, is used. Here the physical processes are simulated which control the penetration and breaking up of individual fragments. To that end the module uses a number of other modules. A short description of the modules is given below.

FAST:

The module which contains the main FAPDS simulation loop.

Init:

The module containing the procedures to initialize the database containing the model of the target and to visualize that model.

Simulate:

The module containing the procedures to perform the FAPDS simulation loop.

Evaluate Event:

This module consists of two modules: *'Evaluate'* and *'Event list'*. The latter contains the procedures to maintain the event list. *'Evaluate'* contains the procedures to evaluate a single event.

Penetrate:

The module containing the procedures to calculate the parameters involved in the penetration process whenever a fragment hits the target.

Thor:

The module containing the (modified) THOR equations to calculate the residual fragment mass and velocity after penetration.

Timelapse:

The module containing the procedures to calculate the time it takes a fragment to perforate the target.

Breakup:

The module containing the procedures to break up a fragment into pieces, with regard to the masses.

Scatter:

The module containing the procedures to scatter the pieces into which a fragment breaks up spatially.

Holes:

The module containing the procedures to deal with the holes created in the target by the fragments.

Shoot ray:

The module containing the procedures to calculate the intersections of the fragment trajectories with the target.

Most of these modules are straight forward implementations of the models discussed in Chapter 3. The *'Evaluate'* module is a more complicated one, because each event in the event list has to be evaluated.

The evaluation of a single event involves the following aspects, as illustrated in Figure B.2. The first step of the evaluation process is to determine whether the fragment flies through a hole. If so, and the fragment is smaller than the hole, the mass and velocity of the fragment remain unaltered and the fragment trajectory (shoot ray) is evaluated further until it hits another part of the target. The collision time is calculated and a new event is added to the event list. If the fragment is larger than the hole, the residual mass and velocity of the fragment is calculated by use of the modified THOR equations. If the fragment is actually capable of perforating the target, the hole is adapted and new vectors for the resulting particles are created.

If no hole is present at the impact point, the next step is to calculate whether the fragment is able to perforate the target. If the fragment is able to perforate the target, the residual mass and velocity are calculated, as well as the location of the exit point and the required perforation time. At the exit point the fragment breaks up and new vectors (in fact trajectories of pieces) are created. For each vector a possible new hit point is determined, and a new event is added to the event list.

REPORT DOCUMENTATION PAGE

(MOD NL)

1. DEFENSE REPORT NUMBER (MOD-NL) TD92-3686	2. RECIPIENT'S ACCESSION NUMBER	3. PERFORMING ORGANIZATION REPORT NUMBER PML1992-128
4. PROJECT/TASK/WORKUNIT NO. 232491308	5. CONTRACT NUMBER A91/KL/422	6. REPORT DATE June 1993
7. NUMBER OF PAGES 48 (2 Annexes)	8. NUMBER OF REFERENCES 9	9. TYPE OF REPORT AND DATES COVERED Final
10. TITLE AND SUBTITLE Description and validation of an improved frangible armour piercing munition model (Beschrijving en validatie van een verbeterd frangible armour piercing model)		
11. AUTHOR(S) T. Keij		
12. PERFORMING ORGANIZATION NAME(S) AND ADDRESS(ES) TNO Prins Maurits Laboratory P.O. Box 45, 2280 AA Rijswijk, The Netherlands		
13. SPONSORING AGENCY NAME(S) AND ADDRESS(ES) DMKL P.O. Box 90822, 2509 LV The Hague		
14. SUPPLEMENTARY NOTES The classification designation: ONGERUBRICEERD is equivalent to: UNCLASSIFIED		
15. ABSTRACT (MAXIMUM 200 WORDS (1044 BYTE)) Frangible Armour Piercing Discarding Sabot (FAPDS) munition is a new type of medium calibre munition for air defense systems. Its penetration behaviour has been studied by TNO-PML in cooperation with BWB, IABG, and Rheinmetall. These studies lead to a simulation model describing the penetration behaviour of 35 mm FAPDS projectiles in thin plate arrays. This report discusses an improved version of the semi-empirical terminal ballistics model for FAPDS munition. With regard to the first simulation model (as reported in report PML 1992-6), the characteristics of the fragmentation process have been changed (use of Mott distribution instead of random distribution, increase in number of particles, and decrease in scattering angle), and the parasitic effect has been described more accurately (effect of hole and particle size on penetration behaviour is included). Due to the changes in the model, the simulation results are consistent with the experimental results. Now, the maximum penetration capacity and the fragment beam width can be calculated accurately for 35 mm FAPDS munition. The influence of the target array composition and the rifling twist of the gun on the simulation results can be predicted well too. However, some problems still have to be solved before the terminal ballistics model can be incorporated into a vulnerability assessment code. The major problem is to find a way to deal with synergistic effects. It is expected that the problems will be solved within the next half year, so that effectiveness calculations can be performed against aircraft and helicopters. The calculation results will be used for the evaluation of several munition types as replacement of today's munition for air defense systems. The replacement probably will take place in 1995.		
16. DESCRIPTORS Penetration Fragmentation Terminal Ballistics		IDENTIFIERS FAPDS
17A. SECURITY CLASSIFICATION (OF REPORT) ONGERUBRICEERD	17B. SECURITY CLASSIFICATION (OF PAGE) ONGERUBRICEERD	17C. SECURITY CLASSIFICATION (OF ABSTRACT) ONGERUBRICEERD
18. DISTRIBUTION AVAILABILITY STATEMENT Unlimited Distribution		17D. SECURITY CLASSIFICATION (OF TITLES) ONGERUBRICEERD

Distributielijst

- 1 DWOO
- 2 HWO-KL
- 3/4 HWO-KLu
- 5 HWO-KM
- 6/8 DMKL-MUN
- 9 DMKL-AB
- 10 DMKL-ArtLua
- 11 DMKL-ARB
- 12/15 BWB-WM IV2, H.Braun (2 x f.a.o. Rheinmetall)
- 16/18 TDCK
- 19 Hoofddirecteur DO-TNO
- 20 Lid Instituuts Advies Raad PML
Prof. drs. P.J. van den Berg
- 21 Lid Instituuts Advies Raad PML
Prof. ir. M.A.W. Scheffelaar
- 22 Lid Instituuts Advies Raad PML
Prof. ir. H. Wittenberg
- 23 PML-TNO, Directeur; daarna reserve
- 24 PML-TNO, Directeur Programma; daarna reserve
- 25 PML-TNO, Divisiehoofd Wapens en Platforms
- 26 PML-TNO, Divisie Wapens en Platforms
Hoofd Groep Wapeneffectiviteit
- 27/28 PML-TNO, Divisie Wapens en Platforms
Groep Wapeneffectiviteit
- 29/31 PML-TNO, Divisie Wapens en Platforms
Groep Ballistiek
- 32 PML-TNO, Documentatie
- 33 PML-TNO, Archief